

Density Collapse and Fluctuation Observed in Poloidally Rotating Plasma on TU-Heliac

Yutaka TANAKA, Sumio KITAJIMA, Mamiko SASAO, Hiroyasu UTOH, Hiroshi AOYAMA, Keisuke IWAZAKI, Hajime UMETSU, Keiichi ISHII, Atsushi OKAMOTO, Takashi KOBUCHI, Shigeru INAGAKI¹⁾, Yasuhiro SUZUKI²⁾ and Hiromi TAKAHASHI²⁾

Department of Quantum Science and Energy Engineering, Tohoku University, Sendai 980-8579, Japan

¹⁾*Research Institute for Applied Mechanics, Kyushu University, Kasuga 816-8580, Japan*

²⁾*National Institute for Fusion Science, Toki 509-5292, Japan*

(Received 16 November 2007 / Accepted 30 March 2008)

The ohmic heated plasma in TU-Heliac was biased by a hot-cathode to drive $\mathbf{E} \times \mathbf{B}$ poloidal rotation. Coincident measurements of the line density and ion saturation currents revealed the existence of density collapse accompanied by fluctuation in the poloidally rotating plasma. The radial density profiles just before and after the collapse were estimated. The steep density gradient vanished with the density collapse. The power spectra of the fluctuation were calculated from the ion saturation current obtained with a high-speed triple probe. The frequency of fluctuation was compared to the $\mathbf{E} \times \mathbf{B}$ poloidal rotation frequency, where the fluctuation appeared with density collapse. The fluctuation frequency was 2 to 3 times the rotation frequency. This suggested that the poloidal mode number of fluctuation was $m = 2$ or 3.

© 2008 The Japan Society of Plasma Science and Nuclear Fusion Research

Keywords: heliac, stellarator, poloidal rotation, density collapse, fluctuation

DOI: 10.1585/pfr.3.S1055

1. Introduction

H-mode was discovered in the ASDEX Tokamak [1] and the mechanism of improvement has been studied extensively since then. Plasma rotation is considered to suppress the anomalous transport. It has also been suggested that plasma turbulence can drive poloidal rotation, such as zonal flow, and that poloidal shock occurs when the poloidal mach number exceeds unity [2]. Therefore, understanding the fluctuation under conditions of plasma rotation, especially in the super sonic regime, is important.

Spontaneous $\mathbf{E} \times \mathbf{B}$ rotation takes place in the improved plasma of large devices. Electrode biasing can drive $\mathbf{E} \times \mathbf{B}$ rotation in a small device resulting in an improved confinement mode. In Tohoku University Heliac (TU-Heliac), negative biasing experiments have been carried out to study the transition to the improved mode [3–11]. A hot cathode made of LaB₆ was used for electron injection into the plasma and a negative potential profile was formed. Typical behaviors of the improved mode were a threefold increase in density and formation of a radial electric field (2–4 kV/m). The $\mathbf{E} \times \mathbf{B}$ poloidal rotation frequency exceeded 100 kHz. At the same time, density and potential fluctuations were observed in low (1–10 kHz) and high (100–1000 kHz) frequency ranges [6, 9, 11]. High frequency fluctuation appeared and disappeared periodically. The frequency of high frequency fluctuation showed radial dependency. In this paper, low frequency fluctua-

tion is understood in terms of a density collapse observed in poloidally rotating plasma, while the characteristics of high frequency fluctuation are described as a burst accompanying density collapse. The high and low frequency fluctuations were measured coincidentally and the frequency of high frequency fluctuation was compared with that of the poloidal rotation. High frequency fluctuation was also measured for four configurations and the dependence on rational surfaces was confirmed.

2. Experimental Setup

TU-Heliac is a helical axis stellarator and forms the heliac configuration. Figure 1 shows the top view of TU-Heliac. The flux surface is formed by the toroidal field coils, the center conductor coil, and the vertical field coils [3]. The heliac configuration has the flexibility of a rotational transform and the magnetic well depth. It is useful to confirm the fluctuation dependence on the configuration in the heliac. The major and minor radii are 48 cm and ~6 cm, respectively. The toroidal period number is 4. A hot cathode was inserted into these flux surfaces at $\phi = 270^\circ$ and a triple probe was inserted at $\phi = 0^\circ$. He gas was selected as the working gas. A plasma was produced by low frequency alternate ohmic heating. The frequency of the heating wave was 18.8 kHz. The plasma current, loop voltage, and power absorbed to the plasma were ~200 A, ~200 V, and ~2 kW, respectively. Typical electron temperature and electron density of the ohmic heated plasma were ~25 eV

author's e-mail: yutaka.tanaka@pp12.qse.tohoku.ac.jp

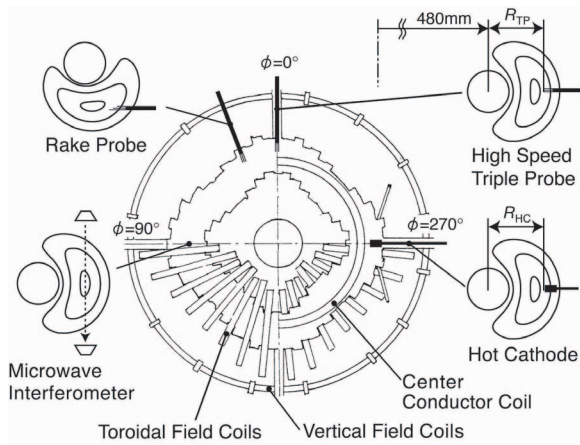
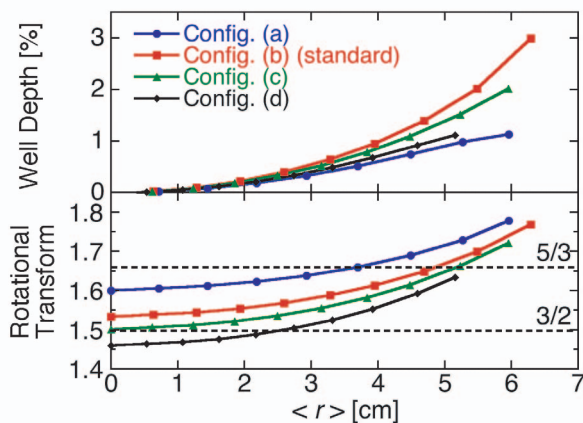


Fig. 1 Top view of TU-Heliac.


 Fig. 2 Radial profiles of the magnetic well depth and the rotational transform in configurations (a)-(d). Configuration (b) was the standard configuration in TU-Heliac. Magnetic field was $B = 0.3$ T in all configurations.

and $6 \times 10^{11} \text{ cm}^{-3}$. The hot cathode was biased against the vacuum vessel. The electrode voltage was fixed at -230 V. The electrode current corresponding the emission current of the hot cathode was about -4 A.

We selected four magnetic configurations. Figure 2 shows the radial profiles of the magnetic well depth and the rotational transform in configurations (a)-(d). Configuration (b) was the standard configuration in TU-Heliac. The magnetic well depth at the last closed flux surface (LCFS), the rotational transform at the magnetic axis, and the magnetic field were 3%, 1.54, and 0.3 T, respectively. Configurations (a), (c), and (d) had high or low rotational transforms as compared to configuration (b); the rotational transforms at the magnetic axis were 1.60, 1.50, and 1.46, respectively. Configurations (a)-(c) had an average minor radius a of ~ 6 cm; a for configuration (d) was ~ 5 cm. In section 3, configuration (b) was used for density collapse and fluctuation measurement. In section 4, all configurations were used comparing the dependence of fluctuation

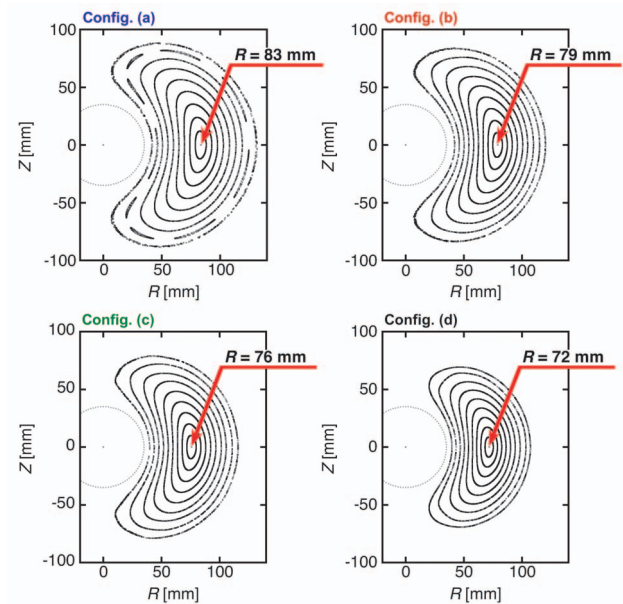


Fig. 3 Flux surface of configurations (a)-(d) shown in Fig. 2. Configuration (b) was the standard configuration in the TU-Heliac. The magnetic axis shifted outward as the rotational transform increased.

on configuration. Figure 3 shows the flux surfaces of these configurations at toroidal angle $\phi = 0^\circ, 90^\circ, 180^\circ,$ and 270° . The circle on the origin is the central conductor coil. The magnetic axis shifts outward as the rotational transform increases. The hot cathode was used for formation of the radial electric field. It could be moved in the R direction on the $Z = 0$ mm plane, where R and Z represent the distance from the center of the central conductor coil as shown in Fig. 3. The top position of the hot cathode was defined by R_{HC} as shown in Fig. 1. In configurations (a)-(d), the hot cathode was set at $R_{\text{HC}} = 90, 86, 83,$ and 79 mm, respectively, which corresponded to 7 mm outside the magnetic axis.

In the hot cathode biased plasma, the $\mathbf{E} \times \mathbf{B}$ poloidal rotation frequency exceeded 100 kHz and the fluctuation frequency reached about 400 kHz by $\mathbf{E} \times \mathbf{B}$ poloidal rotation. A high-speed fluctuation measurement system (cutoff frequency ~ 1 MHz) was required [11]. In this study, high-speed fluctuation measurement and the triple probe measurement were integrated in the high-speed triple probe (HSTP), which was installed in TU-Heliac. The top position of the HSTP was defined by R_{TP} , and could be moved in R direction on the $Z = 0$ mm plane. HSTP was scanned radially across the magnetic axis. A rake probe was inserted at $\phi = 21^\circ$. The rake probe had 3 tips, which were set radially. The distance between the top and bottom tips was 6.0 mm. The 50 GHz microwave interferometer was set at $\phi = 90^\circ$. The rake probe and interferometer were used for coincident measurement of the ion saturation current fluctuation and line density.

3. Density Collapse Accompanied by Fluctuation

The characteristics of hot cathode biased plasma were studied using the HSTP, rake probe, and interferometer. We selected configuration (b), which was the standard configuration in TU-Heliac. The radial positions of the HSTP and the rake probe were calibrated using an electron gun in the configuration without plasma production. This process was important because TU-Heliac has a three-dimensional flux surface. These probes were set at $\rho \sim 0.2$, where ρ was the normalized minor radius defined by $\rho = \langle r \rangle / a$, and $\langle r \rangle$ was the average radius of the flux surface and a was the average minor radius. $\rho = 0.2$ corresponded to the HSTP position $R_{TP} = 87$ mm. The hot cathode was set at $R_{HC} = 86$ mm and biasing experiments were carried out. Figures 4 (a)-(d) show the typical time traces of the plasma current, the electrode voltage, the electrode current, and the ion saturation current. The plasma current was measured with a Rogowski coil and it indicated that the plasma was produced by alternate ohmic heating. The plasma production and hot cathode biasing were started at time = 0 ms and ended at time = 10 ms. The radial electric field and the $\mathbf{E} \times \mathbf{B}$ poloidal rotation were formed by biasing. The plasma current settled into a steady state at time = 1 ms. The electrode current and ion saturation current almost settled into a steady state at 2 ms. These observations suggested that the confinement time was about 1 ms. Figure 4 (e) shows the expanded graph of the line density $n_e l$ and the ion saturation current I_s for 8-9 ms. The ion saturation current was measured by the HSTP and rake probe. The ion saturation current decreased suddenly on the timescale of 0.01 ms (e.g., time = 8.50, 8.65, and 8.81 ms). After the sudden decrease, it increased slowly on the timescale of 0.1 ms. The line density synchronized with the ion saturation current. The ion saturation current is proportional to the density and the root of electron temperature. Increases and decreases in the ion saturation current indicated changes in the density. A sudden decrease in density was observed in different toroidal and radial positions. Therefore, this phenomenon is considered as the density collapse. The line density did not show the fast timescale change of 0.01 ms. This timescale was much smaller than the confinement time. These observations suggested that particles were confined inside LCFS when the density collapse occurred. As line density was integrated density along the central chord, it did not show the fast timescale change. Fast timescale fluctuation was observed in the ion saturation current. This fluctuation burst and simultaneously exhibited similar characteristics in all ion saturation current signals. It did not appear in the phase of density increase after density collapse (e.g., time = 8.50-8.60 ms and 8.65-8.70 ms). These observations suggested that the growth rate of the fluctuation has density or density gradient dependence. The fluctuation grew about 10 μ s as shown in Fig. 4 (f). Then, the growth rate of fluctuation

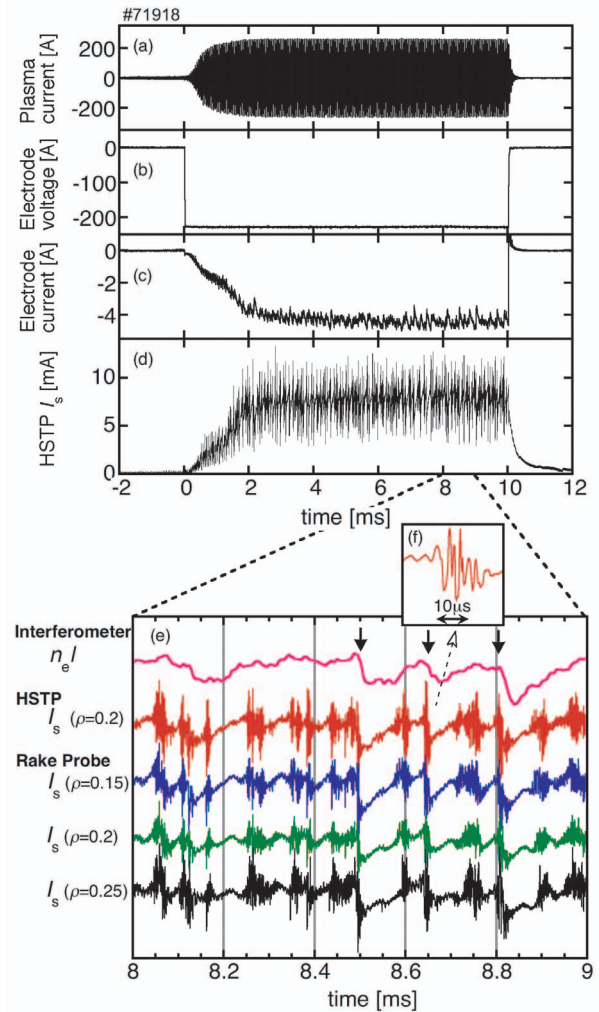


Fig. 4 Typical time traces of (a) the plasma current, (b) electrode voltage, (c) electrode current, and (d) ion saturation current I_s . (e) The line density $n_e l$ and the ion saturation current I_s during the period of 8-9 ms. (f) Expanded graph at 8.65 ms. HSTP and the rake probe were set at $\gamma \sim 0.2$.

could be estimated as $\gamma \sim 10^5 \text{ s}^{-1}$. The growth rate, such as the drift wave instability, was estimated from the dispersion relation for TU-Heliac plasma [6]. The drift wave instability had $\gamma \sim 10^{3-4} \text{ s}^{-1}$. Therefore, the growth rate observed in the biased plasma was extremely large compared to the drift wave instability.

Power spectra were calculated from the ion saturation current I_s and the floating potential V_f obtained by the HSTP as shown in Fig. 5. Fast Fourier transform was used in the calculation. Considering the timescales of the density collapse and density increase, which was observed just after density collapse, the frequency range corresponding to density collapse and density increase was 1 to 80 kHz. The large power of floating potential in this range indicated that the electron temperature or space potential also collapsed with the density collapse because the floating poten-

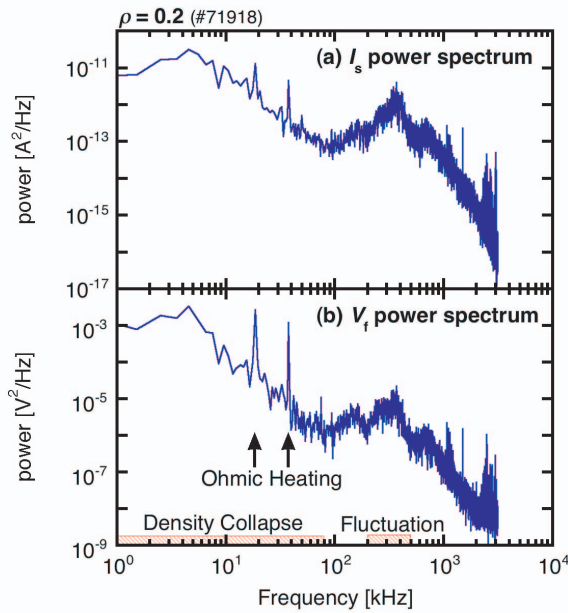


Fig. 5 Power spectra of (a) the ion saturation current I_s and (b) the floating potential V_f . Probe position was $r = 0.2$.

tial was determined by the electron temperature and space potential. The frequency of fluctuation observed in Fig. 4 was 200-500 kHz. The sharp peaks at 18.8 and 37.6 kHz were fundamental and second harmonic oscillations of alternate ohmic heating, respectively. The effects of alternate ohmic heating for the density collapse and bursting fluctuation have not yet been understood. It might be possible to trigger density collapse and bursting fluctuation. The peak at 3 MHz was the noise of the isolation amplifier.

The radial density profile at the moment when the collapse occurred was required to understand the collapse. However, it could not be measured by the diagnostic system in TU-Heliac. Therefore, the radial position of the HSTP was moved in small increments. Ion saturation current data were obtained by changing the position in increments of 1 mm. A digital low pass filter of 18.0 kHz was used to remove the 18.8 kHz ohmic heating oscillation and to pick up only the frequency corresponding to the collapse. Figure 6 shows the radial profile of the ion saturation current obtained by 47 shots. The magnetic axis corresponded to $R_{TP} = 79$ mm and LCFS corresponded to $R_{TP} = 120$ mm. From this figure, it was possible to estimate the density profile at the moment when the collapse occurred. The maximum and minimum lines in the ion saturation current indicated the density profiles before and after the collapse, respectively. Before the collapse, there was a steep gradient in $R_{TP} = 83$ -90 mm. After the collapse, the ion saturation current decreased by about 40% in $R_{TP} = 76$ -87 mm and the steep gradient disappeared. These results suggested that the density gradient triggered the collapse.

The radial profile of the power spectra was obtained

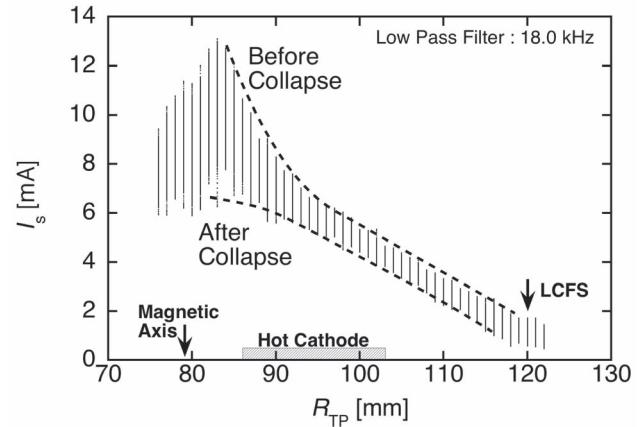


Fig. 6 Radial profile of the ion saturation current obtained by HSTP. Low pass filter of 18.0 kHz was used to remove the 18.8 kHz ohmic heating wave.

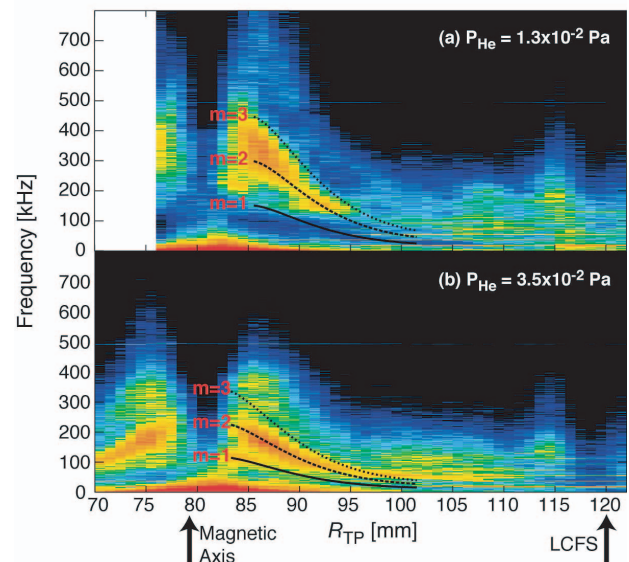


Fig. 7 Radial profiles of the power spectra calculated from the ion saturation current at working gas pressure (a) $P_{He} = 1.3 \times 10^{-2}$ Pa, (b) $P_{He} = 3.5 \times 10^{-2}$ Pa. The lines show the poloidal rotation frequency calculated by Eq. (1). The arrows indicate the magnetic axis and LCFS.

as shown Fig. 7 (a). Working gas pressure was $P_{He} = 1.3 \times 10^{-2}$ Pa. The magnetic axis and LCFS corresponded to $R_{TP} = 79$ and 120 mm. The narrow band mode of the fluctuation was clearly observed in the radial position $R_{TP} = 85$ -95 mm, where the density gradient before the collapse was steep, and in the frequency range 100-500 kHz. This mode corresponds to the fluctuation in the frequency range of 200-500 kHz as shown in Fig. 5. The frequency of this mode showed radial dependence. We considered the fluctuation might depend on the poloidal rotation. Then, the fluctuation frequency was compared to the poloidal rotation frequency. The $\mathbf{E} \times \mathbf{B}$ poloidal rotation frequency f_{EB} was estimated from the radial profile of

the floating potential V_f and was written as

$$f_{EB} = \frac{1}{2\pi\langle r \rangle} \frac{E_r}{B_\phi} = \frac{dV_f/d\langle r \rangle}{2\pi\langle r \rangle B_\phi}, \quad (1)$$

where B_ϕ is the toroidal magnetic field and E_r is the radial electric field. The floating potential was adopted in Eq. (1) instead of the space potential because the error in the latter measured by the HSTP was too large at $R_{TP} = 80\text{-}90$ mm and it could not be used for the calculation. This suggested that the size of the HSTP (4.6 mm) was comparable to the radius of the flux surface at $R_{TP} = 80\text{-}90$ mm. Equation (1) approximately represents the poloidal rotation dependence on the radial position because it largely depends on $\langle r \rangle$ in the denominator. The frequency of mf_{EB} was calculated and plotted in Fig. 7 (a), where m is a positive integer. The poloidal rotation frequency was indicated by the $m = 1$ line. It increased as it approached the magnetic axis and reached about 150 kHz. The radial profile of the fluctuation resembled the $m = 2\text{-}3$ line. To estimate the validity of the comparison between the fluctuation frequency and poloidal rotation frequency, it is important to compare the fluctuation frequency with the poloidal rotation frequency in plasma with different poloidal rotation speeds. One method to change the poloidal rotation speed is to control the working gas pressure. The poloidal momentum balance between the $\mathbf{J}_r \times \mathbf{B}$ driving force, ion viscosity, and ion friction determines the poloidal rotation speed. Increases in the pressure of working gas are connected to increases in ion friction because the friction results from charge exchange between ions and neutral particles. Then, the ion saturation current fluctuation was measured at a working gas pressure $P_{He} = 3.5 \times 10^{-2}$ Pa, which was 2.7 times the gas pressure in our previous experiment. The radial profile of the power spectra was calculated as shown in Fig. 7 (b). The fluctuation was observed in $R_{TP} = 85\text{-}95$ mm and in the frequency range 50-250 kHz. It showed symmetry against the magnetic axis. There was a hole in the fluctuation on the magnetic axis, in which fluctuation did not exist. The poloidal rotation frequency was also calculated and plotted in Fig. 7 (b). The poloidal rotation frequency was about 60% of the rotation frequency in the previous experiment. The radial profile of the fluctuation resembled the $m = 2$ line. Fig. 7 (a) lacks the high field side spectra. The HSTP was inserted from the low field side and the measurement of the high field side was restricted by disturbance from the probe to the plasma.

The radial profile of fluctuation frequency showed good agreement with the $m = 2\text{-}3$ line in both gas pressure conditions. This phenomenon could be explained by the markedly faster $\mathbf{E} \times \mathbf{B}$ rotation velocity than the fluctuation phase velocity determined by the dispersion relation. The physical meaning of m was the fluctuation poloidal mode number, which was estimated to be $m = 2$ or 3. It also showed a surprising result. The fluctuations burst simultaneously in different radial positions as shown in the rake probe in Fig. 4 (e). On the other hand, the fluctuation

frequency was dependent on the radial position.

4. Configuration Effect for Fluctuation

We selected four magnetic configurations for the experiment as shown in Fig. 2. From the results in the previous section, the fluctuation poloidal mode number was estimated to be $m = 2$ or 3. Configuration (b) had the rotational transform 1.5-1.8. The rational surfaces of $m = 2, 3$ were $n/m = 3/2, 5/3$, respectively, where n was the toroidal mode number. Then, configurations (a), (c), and (d) were selected to shift these rational surface positions by changing the rotational transform. TU-Heliac can form a magnetic well configuration, which is considered to stabilize fluctuations. The magnetic well depth at LCFS was 1-3% in these configurations. It is important to produce the same target plasma for comparison. Plasma parameters, such as density and temperature, are dependent on the plasma volume and magnetic field. These configurations had almost the same average minor radius $a = 5\text{-}6$ cm and the same magnetic field at the magnetic axis $B = 0.3$ T. The average density was about $2 \times 10^{12} \text{ cm}^{-3}$ in configuration (a)-(c) and about $1.5 \times 10^{12} \text{ cm}^{-3}$ in configuration (d). Electron temperature was 15-20 eV in all configurations. The magnetic axis shifted inward as the rotational transform decreased. Then, the radial position of the hot cathode R_{HC} was set 7 mm outside the magnetic axis. In configurations (a)-(d), positions were $R_{HC} = 90, 86, 83,$ and 79 mm, respectively. The ion saturation current and the floating potential fluctuations were measured by the HSTP in four configurations and the power spectra were calculated as shown in Fig. 8. Red, green, blue, and black arrows indicate positions of the magnetic axis, the 3/2 rational surface, the 5/3 rational surface, and LCFS, respectively. The He working gas pressure was $P_{He} = 1.3 \times 10^{-2}$ Pa. The ion saturation current spectra in configuration (b) were the same as shown in Fig. 7 (a). The fluctuation can be divided into 3 types: (I) *core fluctuation*, (II) *intermediate fluctuation*, and (III) *edge fluctuation*. These fluctuation positions are shown by dashed circles in all figures. Fluctuation names are also shown in configuration (b). Core fluctuation was observed at $R_{TP} = 83\text{-}95$ mm in the ion saturation current and at $R_{TP} = 83\text{-}90$ mm in the floating potential. The core fluctuation frequency was 100-500 kHz and increased as R_{TP} approached the magnetic axis. Intermediate fluctuation was observed at $R_{TP} = 90\text{-}105$ mm in the floating potential. The intermediate fluctuation frequency was 100-200 kHz and had a flat radial profile. Edge fluctuation was observed just inside LCFS at $R_{TP} = 105\text{-}120$ mm in the floating potential. The fluctuation discussed in the previous section (Fig. 7) was the core fluctuation. There were no clear relation between 3/2 or 5/3 rational surfaces and the core or intermediate fluctuation. Then, it may depend on the rotational transform. In configuration (c), which had the 3/2 rational surface near the magnetic axis and the core

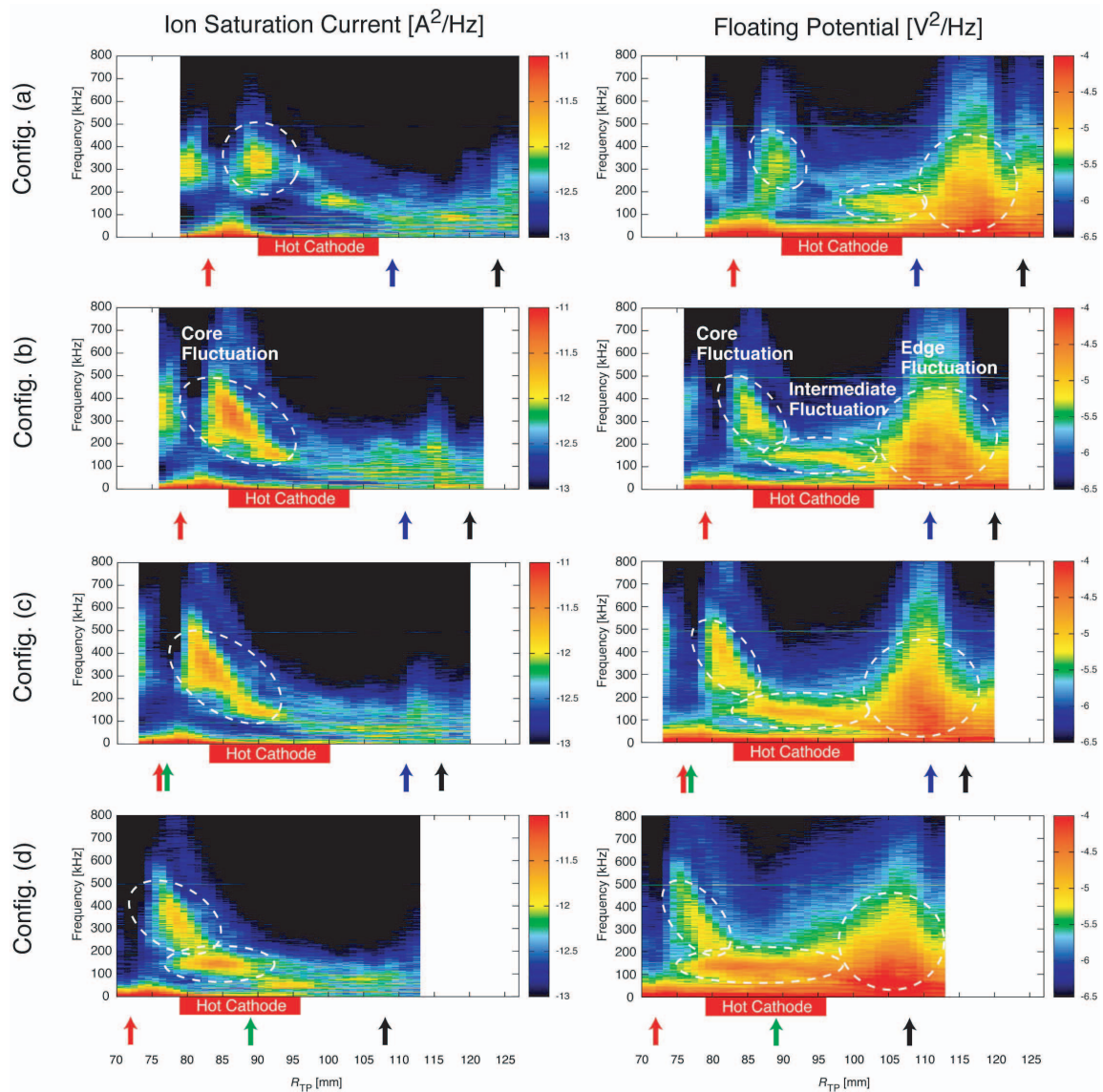


Fig. 8 Radial profiles of power spectra calculated from the ion saturation current and floating potential. The data were obtained by the HSTP in configurations (a)-(d) as shown in Fig. 2. Red, green, blue, and black arrows indicate positions of the magnetic axis, the 3/2 rational surface, the 5/3 rational surface, and LCFS, respectively. In configurations (a)-(d), the hot cathode was set at $R_{HC} = 90, 86, 83,$ and 79 mm, respectively.

fluctuation region, the power of core fluctuation was the same as the power in configuration (b) and larger than the power in configurations (a) and (d). In configuration (d), which had the 3/2 rational surface in the intermediate fluctuation region, the power of intermediate fluctuation was largest compared to the power in the other three configurations. Intermediate fluctuation spread to the core fluctuation region. Intermediate fluctuation of the ion saturation current was also observed and it existed just inside the 3/2 rational surface. These results suggested that intermediate fluctuation was dependent on the 3/2 rational surface and that the mode number was $n/m = 3/2$. In configuration (a), which had the 5/3 rational surface near the intermediate fluctuation region and had a shallow magnetic well, both core fluctuation and intermediate fluctuation were smaller

than in the other configurations. This result suggested that neither the core fluctuation nor the intermediate fluctuation were dependent on the 5/3 rational surface and that the magnetic well effect was negligible compared to the rotational transform effect. Edge fluctuation did not show clear dependence on the configurations and it had a wide spread from 0 kHz to 500 kHz. These characteristics of edge fluctuation were different from those of core and intermediate fluctuations. Figure 9 shows the decrease in ion saturation current ΔI_s at density collapse. The ion saturation current measured at a distance of 7 mm from the magnetic axis was selected and a low pass filter of 18.0 kHz was used in the calculation. ΔI_s was large in configurations (b) and (c) and small in configurations (a) and (d). The collapse dependence on the configuration resembled the core fluctuation

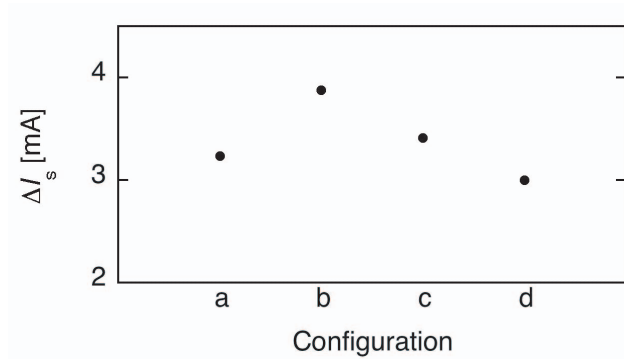


Fig. 9 Decrease of ion saturation current DIs at density collapse. Ion saturation current measured at a distance of 7 mm from the magnetic axis was selected. Low pass filter of 18.0 kHz was used in the calculation.

dependence. The collapse may depend on the core fluctuation.

5. Summary

A hot cathode biasing experiment was carried out in TU-Heliac. Coincident measurements of the line density and the ion saturation currents revealed density collapse accompanied by fluctuation in the poloidal rotating plasma. The power spectra were calculated from the ion saturation current and the floating potential obtained with the high-speed triple probe. The frequency corresponded with a density collapse, and the density increase after the density collapse was 1-80 kHz. The fluctuation frequency was 200-500 kHz. The steep density gradient vanished with a density collapse, and the radial profile of the ion

saturation current fluctuation was obtained and the fluctuation frequency was compared to the $\mathbf{E} \times \mathbf{B}$ poloidal rotation frequency. The fluctuation frequency was 2-3 times the $\mathbf{E} \times \mathbf{B}$ poloidal rotation frequency. These observations suggested that the poloidal mode number was $m = 2$ or 3. The ion saturation current fluctuation and the floating potential fluctuation were measured in four configurations and the experimental results showed that the fluctuation could be classified into *core fluctuation*, *intermediate fluctuation*, and *edge fluctuation*. Core fluctuation corresponded to the fluctuation observed in the density collapse region. Intermediate fluctuation showed the dependence on the $n/m = 3/2$ rational surface position. Therefore, the intermediate fluctuation mode number was considered to be $n/m = 3/2$.

Acknowledgments

This work was supported by a Grant-in-Aid from the Ministry of Education, Science and Culture of Japan (No. 17360439).

- [1] F. Wagner *et al.*, Phys. Rev. Lett. **49**, 1408 (1982).
- [2] R.D. Hazeltine *et al.*, Phys. Fluids **14**, 361 (1971).
- [3] S. Kitajima *et al.*, Nucl. Fusion **46**, 200 (2006).
- [4] H. Takahashi *et al.*, Plasma Phys. Control. Fusion **48**, 39 (2006).
- [5] S. Kitajima *et al.*, Plasma Phys. Control. Fusion **48**, A259 (2006).
- [6] Y. Tanaka *et al.*, Plasma Phys. Control. Fusion **48**, A285 (2006).
- [7] S. Kitajima *et al.*, Fusion Sci. Technol. **50**, 201 (2006).
- [8] H. Takahashi *et al.*, Fusion Sci. Technol. **51**, 54 (2007).
- [9] Y. Tanaka *et al.*, Trans. Fusion Sci. Technol. **51**, 265 (2007).
- [10] M. Ogawa *et al.*, Trans. Fusion Sci. Technol. **51**, 268 (2007).
- [11] Y. Tanaka *et al.*, Plasma Fusion Res. **2**, S1090 (2007).